Research Square

Preprints are preliminary reports that have not undergone peer review.
They should not be considered conclusive, used to inform clinical practice,
or referenced by the media as validated information.

Enhancing the Durability of Roller-Compacted Concrete Dams through Mix Design Optimization Using Fuzzy Taguchi and Response Surface Methods

Esmat Azariun
Islamic Azad University
Mahdi Momeniroghabadi
30902317l9@iau.ir

Islamic Azad University
Mohammad Ali Kazerooni
Islamic Azad University
Roya Amirid
Islamic Azad University

Research Article

Keywords: Roller-compacted concrete dam, lift joint, bedding mortar, placement interval, fuzzy Taguchi method, multi-response performance index, response surface methodology, permeability

Posted Date: November 23rd, 2026

DOI: https://doi.org/10.21203/rs.3.rs-11422301/v1

License: This work is licensed under a Creative Commons Attribution 4.0 International License.
Read Full License

Additional Declarations: No competing interests reported.

Enhancing the Durability of Roller-Compacted Concrete Dams through Mix Design Optimization Using Fuzzy Taguchi and Response Surface Methods

Esmat Azariun[a], Mahdi Momeniroghabadi[* b], Mohammad Ali Kazerooni[c], Roya Amirid[d]

[a] Department of Civil Engineering, Ke,C., Islamic Azad University, Kerman, Iran.
azariunesmat@gmail.com . 0009-0005-8443-4731

[b] Department of Civil Engineering, Ke,C., Islamic Azad University, Kerman, Iran.
3090231719@iau.ir. 0000-0002-2140-2899

[c] Department of Civil Engineering, Ke,C., Islamic Azad University, Kerman, Iran.
kazerooni.ma@iau.ac.ir . 0000-0002-5201-8857
[d] Department of Civil Engineering, Ke,C., Islamic Azad University, Kerman, Iran.
roya.amiri400@yahoo.com

Abstract

Horizontal lift joints are the weakest links of roller-compacted concrete (RCC) dams: they govern interlayer tensile and shear resistance and act as preferential seepage paths, yet mix proportioning practice still treats the RCC body, the bedding mortar and the placement schedule as separate decisions. This study proposes a two-stage, joint-oriented optimization framework in which a fuzzy-logic-based Taguchi analysis (fuzzy multi-response performance index, MRPI) first screens the design space and Response Surface Methodology (RSM) combined with desirability functions then refines the optimum. A 3^3 full-factorial programme (27 combinations plus three replicates; 30 runs and 300 specimens) was executed with RCC cementitious contents of 120, 160 and 200 kg/m^3 (30% fly ash), bedding-mortar cement contents of 250, 400 and 550 kg/m^3, and second-lift placement intervals of 2, 12 and 48 h, i.e., before initial set, after initial set and after final set. Compressive, direct tensile and direct shear strengths and three permeability indices were measured at 90 days. Placement interval was the dominant factor for joint tensile strength ($F = 267.3$): jointed specimens retained about 90% of the monolithic tensile strength at 2 h, 84% at 12 h and less than 60% at 48 h, and the Mohr–Coulomb cohesion of hot joints was on average 88% higher than that of cold joints while the friction coefficient remained practically constant. Raising the RCC cementitious content from 120 to 200 kg/m^3 lowered the permeability coefficient of unjointed concrete by about 90% (from $\approx 45\times10^{-11}$ to $<5\times10^{-11}$ m/s), and the richest bedding mortar reduced joint permeability by about 85% relative to the leanest one. The fuzzy MRPI attributed 59.3%, 23.2% and 11.2% of the multi-response

variation to RCC cementitious content, placement interval and mortar cement content, respectively, and showed that the 400 kg/m^3 mortar performs as well as the 550 kg/m^3 mortar (MRPI = 0.818 vs. 0.817). Second-order RSM models (R^2 = 0.96–0.99) predicted independent validation tests within 1.4–12.3%. The minimum-cement combination that satisfies all dam design targets is an RCC with 160 kg/m^3 cementitious material, a bedding mortar with 400 kg/m^3 cement and placement of the next lift within 2 h (12 h as an upper limit), providing a quantitative basis for joint-oriented specification of RCC dams.

Keywords: Roller-compacted concrete dam; lift joint; bedding mortar; placement interval; fuzzy Taguchi method; multi-response performance index; response surface methodology; permeability.

---

1. Introduction

Roller-compacted concrete (RCC) has become a widely adopted technology for concrete gravity dams because it combines the economy and rapid placement of earthfill construction with the structural performance of mass concrete [3, 5, 11, 23]. Zero-slump concrete is spread in thin lifts (typically 0.3 m) and compacted by vibratory rollers, which reduces the consumption of cementitious material and shortens construction schedules [3, 23, 24]. The price of this layer-by-layer construction is that a large dam contains hundreds of horizontal lift joints (layer zones), and recent studies consistently identify these joints, rather than the parent concrete, as the controlling planes for deformation, sliding stability and seepage [13, 23–25]. Long-term durability against water infiltration, leaching and chemical attack therefore depends to a large extent on the quality of the joints [5, 12, 20, 23].performance of mass concrete [1–3, 11]. Zero-slump concrete is spread in thin lifts (typically 0.3 m) and compacted by vibratory rollers, which eliminates most formwork, reduces the cementitious content and shortens construction schedules substantially [3, 22, 23]. The price of this layer-by-layer construction is that a large dam contains hundreds of horizontal lift joints, and design manuals consistently identify these joints, rather than the parent concrete, as the controlling planes for sliding stability, tensile cracking and seepage [22–24]. Long-term durability against water infiltration, leaching, freeze–thaw cycles and chemical attack therefore depends to a large extent on the quality of the joints [4, 5, 12, 20].

Experimental evidence on the weakness of lift joints is extensive and has been confirmed by recent studies. Bayqra et al. showed that delaying the second layer by 180 min reduced the splitting tensile and compressive strengths of untreated control mixtures by 31% and 17%, respectively, whereas mixtures with interlayer bedding mortar lost only 9% and 10%, and that bedding mortar also reduced water permeability by 59% relative to the control, making it the most effective of the three treatments examined [22]. Hao et al. reported from large-scale field blocks that interlayer tensile strength decreases as the exposure time of the lower layer increases from 4 to 62 h, that the interlayer is weakest between the initial and final set, and that cement slurry or mortar treatment and surface roughening improve bonding [23]. Han et al. showed that the layer zone is a weak, transversely isotropic zone whose presence increases the computed horizontal and vertical displacements of a 215 m high RCC dam by about 25% [24], and Ramadan et al. emphasized the detrimental effect of weak interlayers on the stability of high RCC gravity dams [25]. Seepage along lift joints is generally recognized as the dominant leakage path of RCC dams [10, 13], and the influence of fly ash, which is used almost universally in dam RCC, on the setting, strength development and joint behaviour of RCC has been examined at replacement levels of up to 60% [15, 22].

Conventional proportioning based on design guidance or empirical trial batching optimizes the RCC body for a single target strength and rarely treats the bedding mortar and the construction schedule as co-design variables. In practice, joint quality is controlled mainly through setting-time or maturity limits applied during construction, and these laboratory-derived limits may not reflect field temperature and exposure conditions [23]. Because material variability, curing conditions and the time-dependent reactivity of the lift surface introduce considerable uncertainty [7, 10, 23], a mixture that satisfies the compressive-strength requirement can still produce joints with insufficient cohesion or excessive permeability [13, 22]. Optimization studies in dam and structural engineering have mostly addressed geometry, temperature control, construction time or single material properties [3, 8, 14, 16–18], and only a few have treated the joint as the object of optimization.

Two families of statistical tools are commonly used to optimize concrete mixtures. RSM fits second-order polynomial models to designed experiments and can locate an optimum inside the experimental domain, including points that were not tested; multiple responses are usually combined through desirability functions, as in recent cementitious mix-design optimizations [26]. Machine-learning surrogates have also been proposed for RCC and other concrete properties [4, 6], but they require large data sets. The Taguchi method uses orthogonal arrays and signal-to-noise (S/N) ratios to identify robust factor levels with few experiments [1, 21, 28, 30], and has been applied to RCC mixtures mainly in pavement and additive- or fibre-modified applications [1, 2, 30]; in its original form, however, it handles only one response at a time and does not provide a continuous model of the response [19, 27]. Multi-response extensions based on grey relational analysis [19, 27] or TOPSIS [9] rely on subjective weights, whereas fuzzy inference provides a transparent way of aggregating conflicting responses through linguistic rules [29]. The fuzzy Taguchi approach, in which normalized S/N ratios are combined by a fuzzy inference system into a single multi-response performance index (MRPI), has been applied to multi-response problems in materials engineering [29] and, in the form of fuzzy TOPSIS, to fibre-reinforced concrete [9], but, to the authors' knowledge, it has not been applied to the interlayer behaviour of RCC dams or combined with RSM in a sequential screening–refinement scheme.

The literature therefore leaves three gaps. First, the three variables that the designer and the contractor actually control at a lift joint, namely the cementitious content of the RCC, the cement content of the bedding mortar and the placement interval relative to the setting times, have rarely been optimized simultaneously against strength and permeability targets. Second, the competing responses (tensile strength and cohesion of the joint versus its permeability) are usually optimized one at a time, which leads to inconsistent recommendations; in the present data, for example, compressive strength favours the richest mortar, whereas cohesion favours the intermediate one. Third, existing studies do not separate the best-performing combination from the most economical combination that still meets explicit dam design targets.

To address these gaps, this study makes the following contributions. (i) A 3^3 full-factorial experimental programme with 300 specimens is used to quantify the individual and interactive effects of RCC cementitious content, bedding-mortar cement content and placement interval on compressive, tensile and shear (cohesion–friction) behaviour and on three permeability indices of jointed RCC. (ii) A two-stage optimization framework is developed in which a fuzzy multi-response Taguchi analysis ranks all combinations through a single MRPI and quantifies the percentage contribution of each factor, and second-order RSM models with desirability functions subsequently locate the optimum within the continuous design space. (iii) The optimum is verified experimentally, and the framework distinguishes the performance-maximizing combination from the minimum-cement combination that satisfies all design targets, yielding an explicit, construction-oriented specification for lift-joint treatment.

The remainder of the paper is organized as follows. Section 2 describes the materials, the experimental design, the test methods and the optimization framework. Section 3 presents and discusses the mechanical and permeability results, the Taguchi, fuzzy MRPI and RSM analyses and their validation. Section 4 summarizes the conclusions, practical recommendations and limitations.

2. Materials and Methods

2.1. Raw Materials

In this study, raw materials were carefully selected to provide optimal conditions for producing durable roller-compacted concrete (RCC). Crushed aggregates with a maximum size of 35 mm were chosen in accordance with the United States Army Corps of Engineers (USACE) standards to enhance matrix compaction and improve mechanical properties and durability. The specific gravity and water absorption of the aggregates were determined according to ASTM standards. The aggregate gradation is presented in Table 1. Type II Portland cement, produced by the Anarak Delijan Cement Factory, was employed due to its compatibility with environmental conditions and favorable mechanical properties. The chemical and physical characteristics of the cement fully complied with ASTM standards. Pozzocrete 100 fly ash, a pozzolanic additive, was utilized to improve durability, reduce permeability, and enhance the long-term strength of the concrete.

Table 1: Aggregate Gradation Used in the Concrete Mix Design

Particle Size (mm)	(35-6 mm)	(6-0 mm)	Coarse Aggregate Composition	Ideal Coarse Aggregate Gradation	Fine Aggregate	Ideal Fine Aggregate Gradation	Combined Coarse and Fine Aggregate
37.5	100	100	100	100			100.00
25	90	100	92.5	90			96.25
19	69	100	76.75	70			88.38
12.5	38	100	53.5	55			76.75
9.5	22	100	41.5	35	100	100	70.75
6.3	5.5	99.5	29	28	100	100	64.50
4.75	1.5	80.5	21.25	22	100	95-100	60.63
2.36	1	36	9.75		84.3	75-95	47.03
1.18	1	17	5		59.5	55-80	32.25
0.6	1	17	5		43.8	35-60	24.40
0.3	1	7	2.5		31.8	24-40	17.15
0.15	1	6	2.25		22.7	12-28	12.48
0.075	1	5	2		15.5	6-18	8.75
Specific Gravity	2.663	2.6					
Water Absorption (%)	1.1	1.8					

2.2. Experimental Program and Mix Designs

A three-factor, three-level full-factorial design ($3^3 = 27$ combinations) was adopted so that all main effects, two-factor interactions and quadratic terms could be estimated without aliasing. The factors and levels were:

RCC cementitious content C1, C2 and C3 = 120, 160 and 200 kg/m^3, selected to give nominal 90-day compressive strengths of 17, 22 and 28 MPa; bedding-mortar cement content M1, M2 and M3 = 250, 400 and 550 kg/m^3; and second-lift placement interval T2, T12 and T48 = 2, 12 and 48 h. Each run is denoted CiMjTk; for example, C2M2T2 refers to the 160 kg/m^3 RCC jointed with the 400 kg/m^3 mortar after 2 h. Three additional replicate runs were performed at the C3M3T48 combination to estimate pure experimental error, giving 30 runs in total. Fly ash replaced 30% of the cement by volume in all RCC mixtures, and the water content was kept constant at 107 kg/m^3. The three interval levels were deliberately anchored to the measured setting times of the RCC mixtures (initial and final setting times of 3 h and 16 h for C1, 4.5 h and 18.75 h for C2, and 6 h and 20 h for C3): the 2 h interval lies before initial set (hot joint), the 12 h interval lies between initial and final set (warm joint), and the 48 h interval lies well after final set (cold joint). Details of the 30 runs are given in Table S1.

2.3. Material Proportioning Procedure for Mix Design

The process of determining the material proportions for the mix design was carried out in nine fundamental steps. First, target compressive strengths of 17, 22, and 28 MPa were set for three mix designs labeled C1, C2, and C3, and corresponding cement contents were selected accordingly. Second, physical properties of the raw materials, such as the specific gravity of Portland cement (3.16) and fly ash (2.41), were established. In the third step, the water content was fixed at 107 kg/m³ based on the maximum aggregate size of 37.5 mm. The fourth step involved calculating the cementitious material quantities for each mix. For mix C1 with a cementitious content of 120 kg/m³, 84.1 kg of cement (volume 0.0266 m³) and 27.5 kg of fly ash (volume 0.0114 m³) were assigned. Mix C2 (160 kg/m³) comprised 112.8 kg cement (0.0357 m³) and 36.9 kg fly ash (0.0153 m³), while mix C3 (200 kg/m³) included 139.4 kg cement (0.0441 m³) and 45.6 kg fly ash (0.0189 m³). These calculations maintained a 70% cement and 30% fly ash ratio to reinforce pozzolanic properties and concrete durability. Steps five and six focused on aggregate gradation with a sand volume fraction of 45% of total aggregates. In step seven, the aggregate volumes were calculated for each mix. For mix C1, the combined volume of cement, fly ash, water (0.145 m³), and estimated air content (1.2%, 0.0099 m³) summed to yield an aggregate volume of 0.8331 m³. Mix C3 presented a similar aggregate volume of 0.8083 m³. Step eight calculated the mortar volume, encompassing cement, fly ash, water, air, and fine aggregates smaller than 4.75 mm. Mortar volumes were 0.622 m³ (62%) for C1 and 0.658 m³ (65%) for C3, both within standard ranges. Finally, step nine determined the paste volume and mortar-to-paste ratio. The paste, including cement, fly ash, water, air, and particles smaller than 75 micrometers, had volumes of 0.2206 m³ (with a paste-to-mortar ratio of 0.375) for C1 and 0.2771 m³ (ratio 0.42) for C3.

2.4. Bedding Mortar Mix Design

The bedding mortar was formulated to improve the bond strength at the horizontal interfaces of roller-compacted concrete layers. Following the PCA guidelines for small dams, the mortar comprised Portland cement, sand, water, and set-retarding admixtures. Design criteria included a slump range of 150–230 mm, maximum aggregate size between 6 and 9.5 mm, minimum cement content of 296 kg/m³, and a maximum of 3% sand passing the No. 200 sieve. The target compressive strengths were 13.8 MPa at 7 days and 17.2 MPa at 28 days. A water-reducing admixture and ASTM C494 Type D retarder were incorporated to extend the initial setting time beyond 3 hours. The use of a bedding mortar at the lift interface is consistent with recent laboratory and field evidence that mortar or cement-slurry treatment improves interlayer bonding and reduces joint permeability [22, 23].

2.5. Specimen Preparation

To comprehensively evaluate mechanical properties and durability, 300 specimens were prepared from 30 mix designs. Each design included three specimens for compressive strength testing, two for direct tensile strength, three for shear strength, and two for permeability tests. In total, 90 compressive, 60 tensile, 90 shear, and 60 permeability specimens were fabricated.

Sample preparation began by mixing raw materials (aggregates, cement, fly ash, and water) in a laboratory mixer. Concrete was cast in two layers into cylindrical molds (100 mm diameter × 200 mm height) for compressive and tensile tests and cubic molds (150 mm × 150 mm × 150 mm) for shear and permeability tests. Roller compaction was performed using an electro-pneumatic hammer according to ASTM C1435, simulating field compaction conditions of RCC dams. Before placing the second layer, the surface of the underlying layer was prepared using a green cutting method to enhance bonding. Specimens were demolded after 24 hours and cured in water at 23 ± 2 °C for 90 days to ensure complete pozzolanic reaction of the fly ash and to improve mechanical and durability properties.

2.6. Testing Methods

- **Vebe Time Test:** Conducted according to ASTM C1170 to evaluate the workability of roller-compacted concrete. The time required for the concrete to be consolidated under vibration inside a cylindrical mold and for the formation of a mortar ring around the specimen was recorded to assess the compaction capability of zero-slump mixtures.
- **Compressive Strength Test:** Cylindrical specimens (100 × 200 mm) were tested after 90 days of curing under axial loading following ASTM C39.
- **Direct Tensile Strength Test:** Cylindrical specimens were subjected to tension at a displacement rate of 0.005 mm/s until failure.
- **Shear Strength Test:** Direct shear tests were performed on cubic specimens under normal stresses of 0.6, 0.8, and 1 MPa. A horizontal load was applied at 2.7 mm/min until failure.
- **Permeability Tests:** To assess RCC durability, three permeability tests were conducted:
    1. **Water Absorption and Permeable Voids:** According to ASTM C642-82, the relative porosity was determined by drying 90-day cured cylindrical specimens, measuring weights at saturated surface dry (m_1) and oven-dry (m_2) conditions, and calculating permeable voids using:

$permeable\ void = \left[\frac{m_1 - m_2}{v}\right] * 100$	(1)

where v is the specimen volume.

    2. **Capillary Water Absorption:** Per ASTM C1585, the rate of moisture ingress into concrete pores was measured. Dry cubic specimens (100 mm^3) were partially immersed to 10% of their height in water. Weights were recorded at specified intervals, and absorption rates (in mm) were plotted against the square root of time.
    3. **Water Permeability under Pressure:** Conducted on cubic specimens after 90 days of curing, samples were sealed with impermeable coatings and subjected to hydraulic pressures ranging from 1 to 5 bar. The steady-state flow rate (M) was used with Darcy's law to calculate the permeability coefficient (K):

$K = \frac{M * L}{A * h}$	(2)

where L is specimen length along the flow, A is the cross-sectional area perpendicular to flow, and h is the hydraulic head.

2.7. Statistical Methods and Optimization

- **Taguchi Method**

The Taguchi method was employed as an effective approach for process optimization and reduction of variability in experimental outcomes. Utilizing orthogonal arrays, this method minimized the required number of experiments while improving the quality and stability of results through the analysis of signal-to-noise (S/N) ratios. Key variables, including cement content of the concrete, cement content of the bedding mortar, and layer placement intervals, were examined at three levels. The S/N ratio, used to evaluate variable performance, was calculated using the following formula:

$S/N = 10 \times log\left(\frac{\Sigma\frac{1}{y^2}}{n}\right)$	(3)

where y_i is the response measured in the i-th repetition and n is the number of repetitions. Equation (3) is the larger-the-better (LB) form, which was applied to compressive strength, tensile strength and cohesion. For the permeability coefficient and the capillary absorption index, the smaller-the-better (SB) form, $S/N = -10\log_{10}[(1/n)\,\Sigma\, y_i^2]$, was applied [21, 28]. In both cases a higher S/N ratio indicates better and more robust performance, and the optimal level of each factor is the one with the highest mean S/N ratio.

- **Response Surface Methodology (RSM)**

Response Surface Methodology (RSM) was applied to model nonlinear relationships between independent variables and response variables. This approach facilitated the prediction of roller-compacted concrete properties such as compressive strength, tensile strength, and permeability without the need for extensive additional testing. Both linear and second-order polynomial models were employed.

The linear regression model is expressed as:

$y = \beta_0 + \beta_1 X_1 + \beta_2 X_2 + \cdots + \beta_n X_n + \epsilon$	(4)

where y is the response variable, βi are regression coefficients, Xi are independent variables, and ϵ\epsilonϵ denotes the model error.

For nonlinear data, the second-order polynomial model is given by:

$y = \beta_0 + \sum_{i=1}^{k} \beta_i X_i + \sum_{i=1}^{k} \beta_{ii} x_i^2 + \cdots \sum_{i} \sum_{j} \beta_{ii} X_i X_j + \epsilon$	(5)

This model captures main effects, quadratic effects and two-factor interactions among the variables. ANOVA at a significance level of 5% was used to assess the significance of each term; non-significant terms were removed by backward elimination, and model adequacy was checked by the coefficient of determination (R^2), the adjusted R^2 and residual analysis. Design-Expert software was used to fit the models and to perform the numerical optimization. For model fitting the factors were expressed in a dimensionless form (the water–cementitious ratio of the RCC and the water–cement ratio of the mortar, and the interval in hours), which is why the optimum in Table 9 is reported in these units.

2.8. Fuzzy Multi-Response Taguchi Analysis

Because the joint tensile strength, the joint cohesion and the permeability coefficient lead to different optimal levels when they are analysed separately, they were aggregated into a single multi-response performance index (MRPI) using a fuzzy inference system, following the fuzzy-inference concept used in multi-response Taguchi studies [9, 29]. Compressive strength was not included in the index because it is

not the governing design criterion at the lift joint and was treated as a constraint in Table 6. The procedure consisted of five steps.

Step 1: the S/N ratio η_{ij} of response j in run i was calculated with the LB form for tensile strength and cohesion and the SB form for permeability. Replicate runs were averaged before analysis. Step 2: the S/N ratios were normalized to the interval [0, 1] so that responses with different units could be combined:

$$x_{ij} = (\eta_{ij} - \min_i \eta_{ij}) / (\max_i \eta_{ij} - \min_i \eta_{ij}) \qquad (5a)$$

Step 3 (fuzzification): each normalized input was described by three triangular membership functions, Low (0, 0, 0.5), Medium (0, 0.5, 1) and High (0.5, 1, 1), and the output MRPI by five triangular functions, Very Small (0, 0, 0.25), Small (0, 0.25, 0.5), Medium (0.25, 0.5, 0.75), Large (0.5, 0.75, 1) and Very Large (0.75, 1, 1). Step 4 (inference): a complete rule base of $3^3 = 27$ rules of the form 'if x_1 is A_{1k} and x_2 is A_{2k} and x_3 is A_{3k}, then MRPI is B_k' was constructed, in which the output class B_k increases monotonically with the sum of the input levels, so that all three responses are weighted equally. The Mamdani max–min compositional operation was used:

$$\mu_B(y) = \max_k \{ \min [\mu_{A1k}(x_1), \mu_{A2k}(x_2), \mu_{A3k}(x_3), \mu_{Bk}(y)] \} \qquad (5b)$$

Step 5 (defuzzification): the crisp MRPI of each run was obtained by the centroid method:

$$\mathrm{MRPI} = \int y\, \mu_B(y)\, dy \,/\, \int \mu_B(y)\, dy \qquad (5c)$$

The mean MRPI of each factor at each level was then computed, the level with the highest mean MRPI was taken as optimal, and the relative importance of each factor was quantified by its percentage contribution:

$$\rho_f = SS_f / SS_T \times 100, \quad SS_f = 9\, \Sigma_l\, (\bar{m}_{fl} - \bar{m})^2 \qquad (5d)$$

where $\bar{m}_{fl}$ is the mean MRPI of factor f at level l, $\bar{m}$ is the grand mean, and SS_T is the total sum of squares of the MRPI over the 27 combinations.

2.9. RSM-Based Desirability Optimization and Experimental Validation

In the second stage, the fitted second-order models were used to search the continuous design space with the desirability approach [26]. Each predicted response $\hat{y}_j$ was transformed into an individual desirability $d_j \in [0, 1]$ according to the goal and limits given in Table 6 (maximize for strengths and cohesion, minimize for permeability, with cement contents minimized for economy), and the composite desirability was maximized:

$$D = (d_1 \times d_2 \times \ldots \times d_k)^{1/k} \qquad (5e)$$

The optimum was verified by casting and testing new specimens at the recommended combination. The prediction error was calculated as $|\hat{y} - y_{exp}| / y_{exp} \times 100$. The overall framework is therefore sequential: the full-factorial tests provide the data, the conventional and fuzzy Taguchi analyses screen the discrete levels and quantify factor importance, and the RSM–desirability stage refines and verifies the optimum.

3. Results and Discussion

This section presents a detailed analysis of the experimental results obtained from 30 roller-compacted concrete (RCC) mix designs. The primary objective is to rigorously investigate the effects of key variables, including concrete cement content, bedding mortar cement content, and the timing of the second layer placement, on the mechanical properties and durability of RCC. Using statistical and mathematical methods, the individual and interactive impacts of these variables on compressive, tensile, shear strength, and permeability are analyzed to identify an optimal mix design suitable for RCC dam applications.

3.1. Compressive Strength

The compressive strength evaluation of jointed RCC samples revealed that several factors, such as concrete cement content, bedding mortar cement content, and layer placement interval, significantly influence the mechanical performance of the structure. Table 2 summarizes the compressive strength results of the concrete and bedding mortar mixes at 7 and 90 days. An appreciable increase in compressive strength was observed with specimen age; notably, mix C3, with the highest cement content (200 kg/m³), demonstrated approximately 2.5 times greater 90-day strength compared to its 7-day strength. A similar trend was observed for the bedding mortars, with mix M3 (550 kg/m³ cement content) exhibiting a higher strength gain rate than the others.

Table 2: Compressive Strength of Concrete Mixes and Bedding Mortars at Different Ages (MPa).

Group	7 days	90 days	Mortar	7 days	90 days
C1	4.60	15.36	M1	10.96	13.37
C2	8.48	21.48	M2	17.69	28.18
C3	11.16	28.34	M3	29.60	39.75

Figure S1 illustrates the effect of different second layer placement intervals (2, 12, and 48 hours) on the compressive strength across 30 distinct mix designs. The results indicated a significant reduction in compressive strength with increasing interval time between the two layers, with a sharper decline observed between 12 and 48 hours compared to 2 and 12 hours. Moreover, the cement content of the bedding mortar directly influenced compressive strength; mortars M2 and M3, having higher strengths than the base concrete, enhanced the compressive strength of the jointed specimens. In contrast, mortar M1, with lower strength than the base concrete, significantly decreased compressive strength. On average, increasing the bedding mortar cement content from M1 to M3 resulted in approximately a 30% increase in compressive strength.

Figure 1 presents the signal-to-noise (S/N) ratio analysis for compressive strength. The analysis revealed that the concrete cement content (indicated by the steepest slope) exerted the greatest influence on compressive strength, followed by the bedding mortar cement content and the layer placement interval. The optimal combination for maximum compressive strength corresponded to level 3 of concrete cement content (C3), level 3 of bedding mortar cement content (M3), and level 1 of layer placement interval (2 hours). However, considering economic and environmental factors, using mortar M2 may be a more viable option, as it does not significantly reduce compressive strength compared to mortar M3.

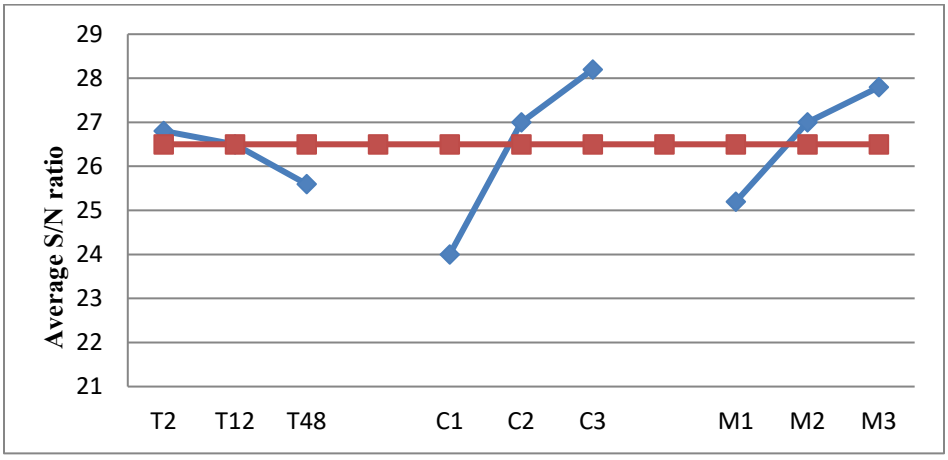


Figure 1: Effect of Variables on Compressive Strength (Signal-to-Noise Ratio Analysis).

3.2. Tensile Strength

Table 3 presents the tensile strength test results of jointed specimens along with the failure mode of each sample. This table provides comprehensive data for 30 different mix designs, with tensile strengths ranging from 0.82 to 2.16 MPa. The direct tensile strength results of non-jointed roller-compacted concrete (RCC) specimens at 90 days for mixes C1, C2, and C3 were 1.52, 1.904, and 2.4 MPa, respectively. The ratio of direct tensile strength to Brazilian tensile strength varied between 0.57 and 0.67, whereas design guidelines typically recommend a value of 0.75. This discrepancy indicates the need for a more detailed investigation into factors such as aggregate gradation and cement paste content in determining this ratio. To evaluate the tensile strength of jointed specimens, various failure mechanisms were examined. Six types of failure were identified: (a) failure within the bedding mortar, (b) failure in the first concrete layer, (c) failure in the second concrete layer, (d) failure at the interfacial transition zone (ITZ) between the mortar and the first layer, (e) failure at the ITZ between the mortar and the second layer, and (f) simultaneous failure across all three regions. The majority of failures were of type (d), i.e., failure at the ITZ between the mortar and the first layer, indicating a weakness in this region within the RCC structure.

Table 3: Tensile Strength Test Results of Jointed Samples.

Group	Tensile Strength (MPa)	Failure Type	Group	Tensile Strength (MPa)	Failure Type
C1M1T2	1.38	b	C2M1T48	1.10	d
C1M2T2	1.43	b	C2M2T48	1.12	d
C1M3T2	1.25	b	C2M3T48	1.20	d
C1M1T12	1.16	d	C3M1T2	1.73	a
C1M2T12	1.23	d	C3M2T2	1.89	b
C1M3T12	1.20	f	C3M3T2	2.16	c
C1M1T48	0.82	d	C3M1T12	1.30	d
C1M2T48	1.10	d	C3M2T12	2.09	c
C1M3T48	1.13	d	C3M3T12	1.50	d
C2M1T2	1.67	a	C3M1T48	1.12	d
C2M2T2	1.66	b	C3M2T48	1.28	d
C2M3T2	1.90	b	C3M3T48	1.37	d
C2M1T12	1.63	a	C3M3T48	1.40	d
C2M2T12	1.55	c	C3M3T48	1.50	d
C2M3T12	1.84	b	C3M3T48	1.37	d

Figure S2 illustrates the relationship between tensile strength and the interval between layer placements. The investigation of the effect of this time interval revealed that with increasing delay between the placement of two layers, surface bonding and tensile strength decrease. This reduction is attributed to the progression of hydration on the surface of the first layer and the decrease in the thixotropic properties of the cement paste, which leads to the formation of a weaker interfacial transition zone between the layers. At 2 hours (before initial setting), the bonding between the two layers is very strong, and the specimen behaves integrally. In this condition, the tensile strength of hot-jointed specimens averages 90% of that of non-jointed specimens. At 12 hours (after initial setting), surface reactivity decreases and tensile strength drops to 84% of that of non-jointed specimens. At 48 hours (after final setting), the joint behaves as a cold

joint, and tensile strength falls below 60% of that of non-jointed specimens. Analysis of the effect of bedding mortar cement content showed that increasing cement content improves tensile strength and bonding between the mortar and underlying concrete. However, this effect is more limited in cold-jointed specimens (48-hour interval). Mortar with 250 kg/m³ cement content (M1) showed poor performance, whereas mortars with 400 and 550 kg/m³ (M2 and M3) were both acceptable. These ratios agree with the strong sensitivity of joint tensile strength to placement delay reported by Bayqra et al. [22], who observed a 31% loss of splitting tensile strength for a 180 min delay without bedding mortar, and with the field finding of Hao et al. that interlayer tensile strength decreases with exposure time and is lowest between the initial and final set [23]. The present results add that the critical threshold is the initial setting time of the lower lift: once it is exceeded, increasing the mortar cement content cannot restore the monolithic tensile strength.

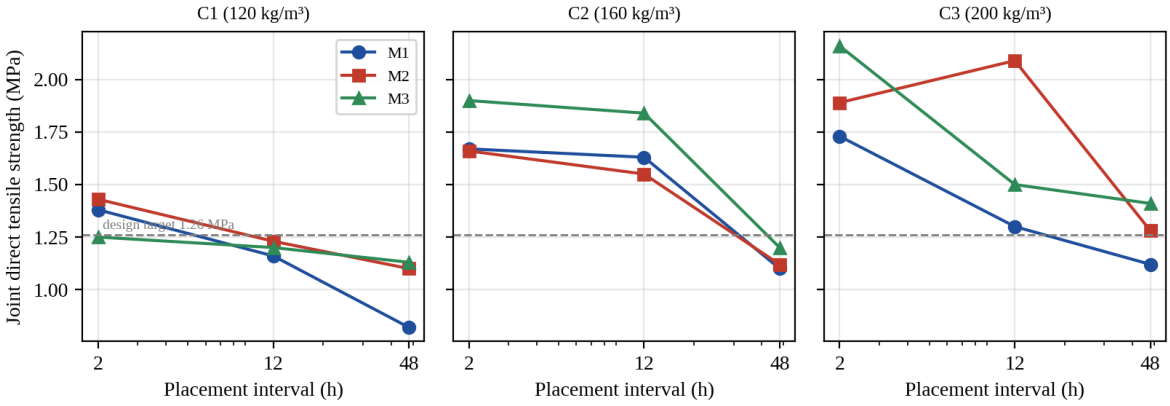


Figure S2: Joint direct tensile strength versus placement interval for the three RCC mixes and the three bedding mortars (data of Table 3; dashed line: design target).

To systematically evaluate the effects of variables, signal-to-noise (S/N) ratio analysis was conducted. Figure 2 presents the results of the S/N analysis for tensile strength. Unlike compressive strength, in tensile strength, the timing of the second layer placement has the greatest influence, followed by the concrete cement content and the cement content of the bedding mortar. This finding highlights the critical importance of precisely controlling the scheduling of layer placement in roller-compacted concrete dam projects. Considering construction costs and environmental concerns, it is recommended to use a mix design with medium cement content (C2), bedding mortar with 400 kg/m³ cement content (M2), and a maximum interval of 12 hours for placing the second layer after the first. This combination maintains acceptable tensile strength while also being economically viable.

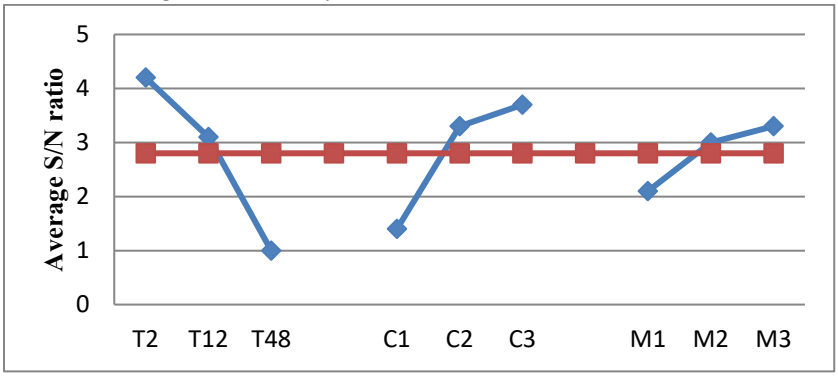


Figure 2: Effect of Variables on Tensile Strength.

3.3. Shear Strength

Shear strength tests under various normal loads revealed that the shear behavior of the joint between two roller-compacted concrete layers is influenced by several factors, including the time interval between layer placements, the cement content of the bedding mortar, and the cement content of the concrete. Figures S3(a) and S3(b) illustrate the relationship between horizontal displacement and joint shear strength. Figure S3(a) shows this relationship for different mortars in C3T48 specimens under a 1 MPa normal stress, while Figure S3(b) compares shear behavior at different time intervals for the C2M2 mix design. The tests demonstrated that with applied load and increasing horizontal displacement, the shear strength gradually rises until reaching the peak shear strength (Qp), after which a sudden drop occurs due to the failure of layer cohesion. Examination of the effect of time interval revealed that increasing the delay between the placement of two layers reduces the shear strength. At 2 hours (before initial setting), the reduction in strength is relatively small as the cement paste is still capable of providing sufficient bonding. However, after the initial set (12 hours), and especially after the final set (48 hours), bonding deteriorates significantly.

Figure 3(a) and 3(b) depict the relationship between maximum shear stress with respect to time interval and bedding mortar cement content, respectively. Figure 3(a) shows the correlation between peak shear strength and varying time intervals under different loads for the C3M2 mix. Results indicate that increasing the time interval from 2 to 12 and then to 48 hours reduces shear strength by approximately 12–13% and 22–24%, respectively. Figure 3(b) illustrates the relationship between bedding mortar cement content and joint shear stress for the C3T2 mix. Analysis of the mortar cement content effect showed that increasing the mortar cement content from M1 (250 kg/m³) to M2 (400 kg/m³) raised the peak shear strength by about 6–7%, whereas the richest mortar M3 gave a lower value than M2 (Table 4; Figure 3(b) is drawn from these data), i.e., the benefit of additional cement saturates at about 400 kg/m³. This is also reflected in the failure mode: in C3M1T2 and C3M3T2 specimens failure occurs within the mortar itself (type a), whereas in C3M2T2 specimens the mortar ceases to be the weakest zone and failure shifts to the interfacial transition zone (type d).

(a)	(b)

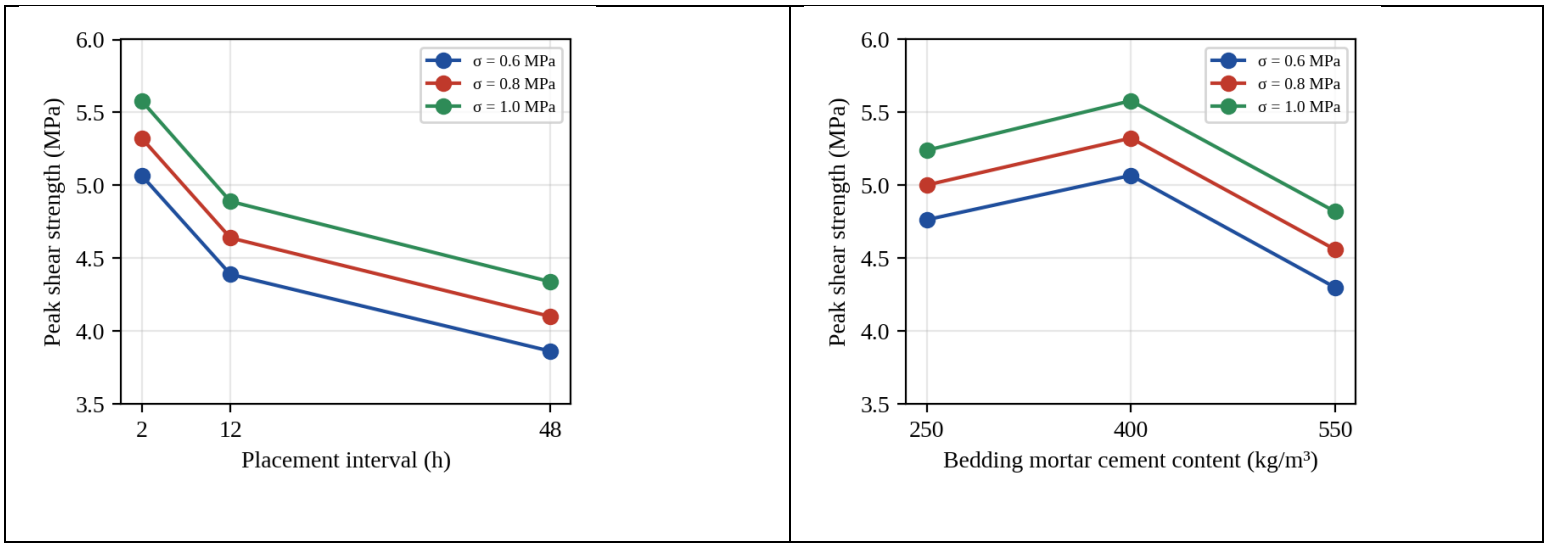


Figure 3: Relationship between Peak Shear Stress, Time Interval, and Bedding Mortar Cement Content.

The failure modes of specimens also vary with the time interval. Figure S4 depicts the different joint shear failure modes. Tests showed that at 2 hours, failure mainly occurs within the mortar (type a) or concrete (type b), indicating good bonding between layers. After initial setting, the failure plane shifts to the interfacial transition zone between the mortar and the first layer (type d), which is the weakest region in the joint. This transition in failure mode directly demonstrates the influence of second layer placement timing on the failure mechanism.

To analyze the shear behavior of joints, the Coulomb failure criterion was used, which expresses the relationship between shear stress (τ), normal stress (σ), coefficient of friction (f), and cohesion (c) as $\tau = f\sigma + c$. Table 4 presents the values of cohesion (c) and friction coefficient (f) for 30 different mix designs. Data analysis revealed that as the tensile strength of the samples increased from 1.5 to 2.3 MPa (transitioning from mix C1 to C3), the friction coefficient (f) remained approximately constant, while the cohesion value (c) increased by more than 1.5 times. This indicates that tensile strength has a significant impact on cohesion, but only a minimal effect on friction. It was also observed that increasing the time interval between layer placements led to a substantial reduction in cohesion. On average, the cohesion value for hot joints (layers placed within short intervals) was 88% higher than that of cold joints. After final setting, the cohesion coefficient was reduced by up to 30%. The nearly constant friction coefficient (≈1.1–1.4) and the strong dependence of cohesion on the bond quality are consistent with field evidence that interlayer treatment and exposure time govern interlayer bonding [23] and that the layer zone is the weak element of RCC dams [24]. This implies that, in sliding stability analyses, the effect of the placement interval should be introduced primarily through the cohesion term rather than through the friction angle.

Table 4: Values of Cohesion (c) and Friction Coefficient (f) for 30 Mix Designs.

Group	Cohesion (c)	Friction Coefficient (f)	Failure Type	Group	Cohesion (c)	Friction Coefficient (f)	Failure Type
C1M1T2	1.87	1.20	a	C2M3T2	2.17	1.14	a
C1M1T12	1.58	1.20	d	C2M3T12	1.98	1.30	d
C1M1T48	1.48	1.20	d	C2M3T48	1.87	1.13	d
C1M2T2	2.26	1.32	b	C3M1T2	4.05	1.19	a

C1M2T12	1.03	1.23	d	C3M1T12	3.35	1.30	d
C1M2T48	1.12	1.70	d	C3M1T48	2.99	1.15	d
C1M3T2	2.63	1.40	b	C3M2T2	4.30	1.28	d
C1M3T12	2.29	1.26	d	C3M2T12	3.64	1.25	d
C1M3T48	1.85	1.19	d	C3M2T48	3.15	1.19	d
C2M1T2	1.95	1.15	a	C3M3T2	3.52	1.30	a
C2M1T12	1.73	1.19	d	C3M3T12	3.46	1.32	d
C2M1T48	1.70	1.20	d	C3M3T48	2.78	1.21	d
C2M2T2	3.12	1.40	b	C3M3T48	2.97	1.38	d
C2M2T12	2.75	1.30	d	C3M3T48	2.82	1.33	d
C2M2T48	2.14	1.16	d	C3M3T48	2.64	1.24	d

To systematically investigate the effect of variables on cohesion, signal-to-noise (S/N) ratio analysis was conducted. Figure 4 presents the results of this analysis. The figure reveals that, in terms of shear strength, the cement content of the bedding mortar has the greatest influence, while the concrete cement content and layer placement interval have a nearly equal but lesser effect. Considering construction costs and environmental concerns, the use of mortar with 250 kg/m³ cement content (M1) is deemed unsuitable. However, both M2 and M3 mortars are considered acceptable. To optimize cost efficiency while maintaining adequate shear strength, the use of M2 is recommended. The optimal combination for achieving maximum shear strength involves placing the second layer within 2 hours of the first, using the highest concrete cement content (C3), and a medium cement content in the bedding mortar (M2). This combination offers a balanced solution that meets mechanical performance requirements while addressing both economic and environmental considerations.

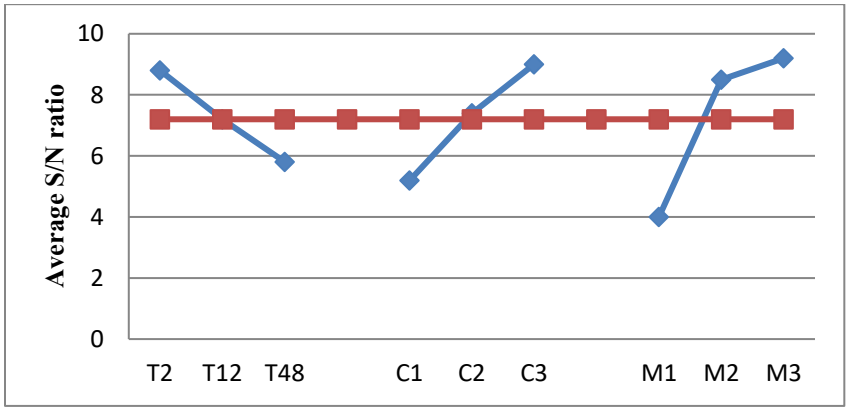


Figure 4: Influence of Various Variables on Cohesion.

3.4. Permeability

Permeability in roller-compacted concrete (RCC) primarily occurs through two main pathways: interconnected pores resulting from compaction and the weak, porous interfacial transition zone between the cement paste and aggregates. This study investigates the influence of concrete cement content, bedding mortar cement content, and the time interval between layer placements on the permeability of RCC. To provide a comprehensive assessment, three different tests were conducted: water absorption and permeable voids, water permeability under pressure, and capillary absorption.

3.4.1. Water Absorption and Permeable Voids Test

Figure 5 illustrates the water absorption behavior of different mix designs. Water absorption was evaluated at two specific intervals-initial absorption after 30 minutes and final absorption after 50 hours. Results showed that the initial surface absorption in mix C1 was approximately 3% lower than in mixes C2 and C3. According to the CEB classification, mix C1 falls under the "good" category, while mixes C2 and C3 are categorized as "average." The figure clearly indicates that as cement content increases from C1 to C3, both initial (30-minute) and final (50-hour) water absorption decrease. This descending trend was consistently observed across all three mix designs, confirming that increasing cement content and reducing the water-to-cement ratio lead to a decrease in pore volume and, consequently, greater resistance to water ingress. The reduced absorption associated with higher cement content is attributed to a denser microstructure and fewer voids, contributing to enhanced concrete durability.

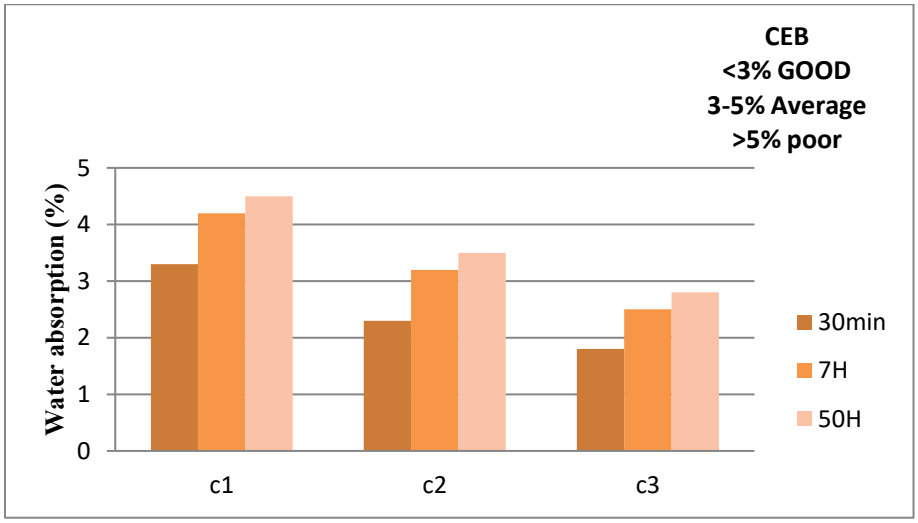


Figure 5: Water Absorption of Different Mix Designs.

Figure S5 illustrates the relationship between water absorption and permeable voids. The permeable voids test revealed a direct correlation between the percentage of water absorption and the volume of permeable pores. As the percentage of permeable voids increases, water absorption also rises significantly. As shown in the figure, an increase in the volume of permeable voids from approximately 8% to 18% corresponds with a rise in water absorption from around 4% to over 9%. The high correlation coefficient of this relationship ($R^2 \approx 0.98$) indicates a strong link between the two parameters. This finding underscores the importance of controlling pore volume to improve concrete performance under varying environmental conditions. It clearly demonstrates that reducing the volume of voids can effectively decrease both water absorption and overall permeability.

3.4.2. Water Permeability under Pressure

In the water permeability test, the volume of water infiltrating the concrete was measured until a steady-state flow rate was achieved. This equilibrium flow rate was typically reached after two days of testing. Figure 6 shows that increasing the cement content from C1 to C3 leads to a significant reduction in the permeability coefficient. For mix C1, with the lowest cement content (120 kg/m^3), the permeability coefficient was approximately 45×10^{-11} m/s, whereas in mix C3, with the highest cement content (200

kg/m³), it dropped to less than 5×10^{-11} m/s. The figure also illustrates that the permeability coefficients of the mortars (M1, M2, and M3) are considerably lower than those of the roller-compacted concrete. As the cement content of the mortar increases from M1 to M3, permeability decreases accordingly. Mortar M3, with a cement content of 550 kg/m³, exhibited the lowest permeability. These results emphasize the critical role of selecting an appropriate cement content in the bedding mortar to minimize joint permeability in RCC structures.

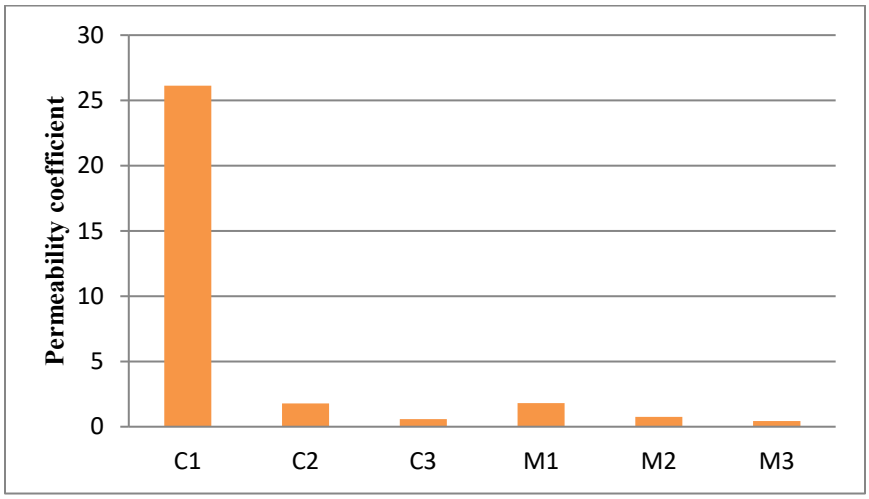


Figure 6: Permeability Coefficient of Non-Jointed Specimens.

Figure S6 provides a more detailed view of how the mortar cement content affects joint permeability in C3T2 specimens. As the mortar cement content increases from M1 (250 kg/m³) to M3 (550 kg/m³), the permeability coefficient decreases from approximately 14×10^{-11} to below 2×10^{-11} m/s—an 85% reduction. This substantial improvement is attributed to the denser structure of hydration products and the enhanced quality of the interfacial transition zone between the mortar and concrete layers. However, the figure also shows that even with the use of M3, the permeability of the jointed specimen remains higher than that of the non-jointed C3 specimen. This finding highlight that the interlayer interface continues to be the primary pathway for water leakage in roller-compacted concrete structures. A comparable benefit of bedding mortar (a 59% reduction in water permeability relative to the control) was reported by Bayqra et al. [22], who also found that the detrimental effect of the cold joint on permeability grows with the delay in placing the second layer. Because lift joints are generally the main seepage path of RCC dams [10, 13], the joint should be regarded as the controlling seepage path in the design of upstream facing and drainage systems.

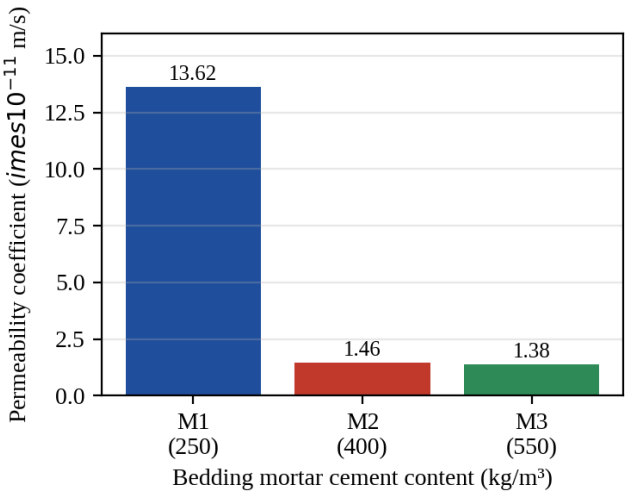


Figure S6: Permeability coefficient of C3T2 jointed specimens as a function of bedding mortar cement content (data of Table 5).

3.4.3. Capillary Water Absorption Test

The permeability coefficient and capillary absorption index of jointed concrete specimens are presented in Table 5. The results of this test are consistent with those of the water permeability test, indicating a direct correlation between the microstructural characteristics of concrete and its resistance to water ingress.

Table 5: Permeability Coefficient and Capillary Absorption Index for 30 Mix Designs.

Group	Permeability Coefficient (10^{-11} m/s)	Capillary Absorption Index	Group	Permeability Coefficient (10^{-11} m/s)	Capillary Absorption Index
C1M1T2	40.1	0.388	C2M3T2	3.57	0.079
C1M1T12	58.9	0.5075	C2M3T12	6.54	0.010
C1M1T48	95.1	0.7	C2M3T48	13.08	0.160
C1M2T2	32.68	0.26	C3M1T2	13.62	0.18
C1M2T12	37.269	0.34	C3M1T12	31.04	0.227
C1M2T48	80.1	0.52	C3M1T48	38.48	0.388
C1M3T2	25.06	0.23	C3M2T2	1.46	0.037
C1M3T12	31.034	0.24	C3M2T12	2.73	0.073
C1M3T48	59.012	0.49	C3M2T48	15.84	0.205
C2M1T2	37.34	0.4	C3M3T2	1.38	0.04
C2M1T12	49.1	0.49	C3M3T12	2.11	0.064
C2M1T48	56.29	0.49	C3M3T48	8.68	0.125
C2M2T2	4.37	0.12	C3M3T48	13.62	0.18
C2M2T12	7.1	0.11	C3M3T48	31.04	0.227
C2M2T48	34.49	0.29	C3M3T48	38.48	0.388

Figure S7 shows the relationship between the capillary absorption index and the permeability coefficient. As depicted, the capillary absorption index increases linearly with the permeability coefficient ($R^2 \approx 0.92$). This strong correlation between the two parameters suggests that both tests effectively assess the concrete's pore structure. At low permeability coefficients (below 10×10^{-11} m/s), the capillary absorption index

remains under 0.15, whereas as the permeability coefficient rises above 90×10^{-11} m/s, the absorption index increases to approximately 0.7. This direct relationship allows for the prediction of one parameter based on the other and can be useful in evaluating the durability of roller-compacted concrete. The close relationship between sorptivity and pressure permeability suggests that the simpler sorptivity test can serve as a quality-control indicator of joint tightness, in the same way that permeability-type indicators (water penetration depth under pressure) have been used to rank joint treatments [22].

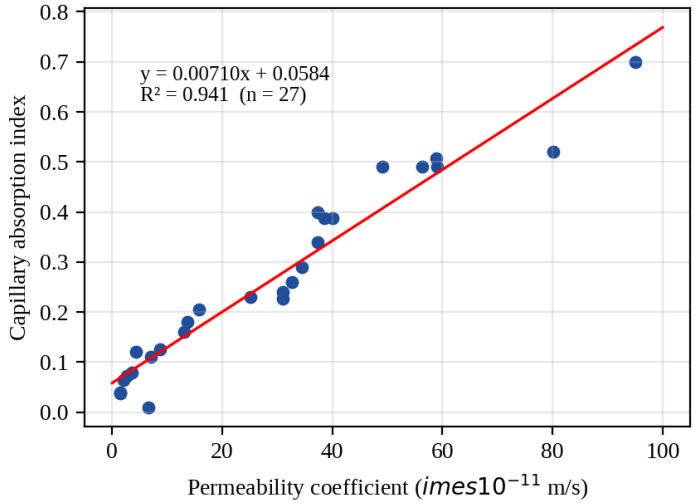


Figure S7: Capillary absorption index versus permeability coefficient of the 27 mix combinations (data of Table 5) with linear regression.

Figure 7 presents the results of the signal-to-noise (S/N) ratio analysis for permeability. Contrary to the compressive and tensile strength results, all three variables exert a significant influence on permeability. The time interval between layer placements displays a steeply declining trend, with the S/N ratio decreasing as the interval increases from 2 to 12 and then to 48 hours. This decline is more pronounced between 12 and 48 hours, indicating that prolonged time intervals adversely increase permeability. The figure also shows that increasing the cement content of the concrete from C1 to C3 raises the S/N ratio, reflecting a reduction in permeability. A similar trend is observed for the cement content of the bedding mortar, where permeability decreases as cement content increases from M1 to M3. The optimal combination for minimizing permeability involves using the highest cement content in concrete (C3), the highest cement content in mortar (M3), and the shortest layer placement interval (2 hours). Unlike compressive strength, where concrete cement content had the greatest effect, and tensile strength, where the timing was the dominant factor, permeability is nearly equally influenced by all three variables. This finding highlights the critical importance of considering all these factors in designing roller-compacted concrete with minimal permeability and underscores the need for a balanced approach to achieve highly durable concrete.

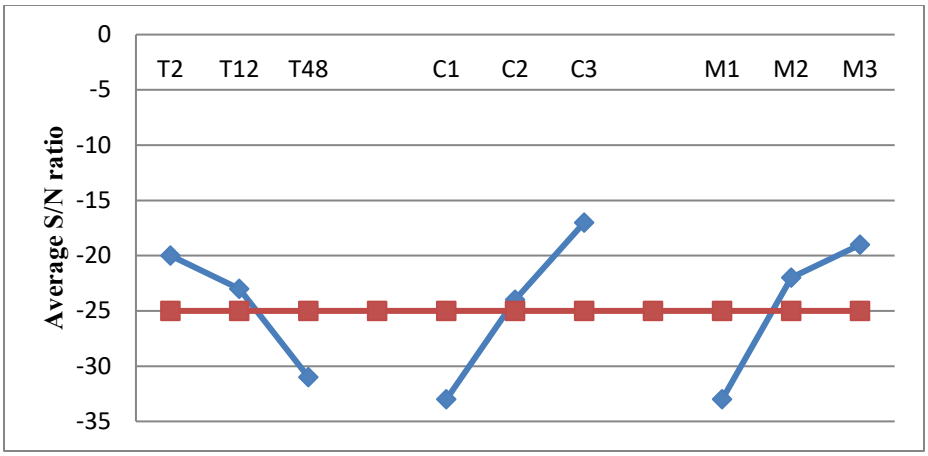


Figure 7: Influence of Variables on Permeability.

3.5. Phase Two: Modeling and Optimal Mix Design Proposal

3.5.1. Obtaining the Optimal Mix Design Using the Taguchi Algorithm

In the design of roller-compacted concrete (RCC) dams, mechanical strength and durability play fundamental roles. One of the key differences between RCC dams and conventional concrete dams is the presence of weak horizontal planes or joints that form during the concreting process. Experimental results revealed that the tensile and shear strengths of these joints are significantly lower than those of the bulk concrete, while the permeability coefficient of the joints can be more than 100 times higher than that of non-jointed specimens. Therefore, special attention must be given to reducing the loss of strength and the increase in permeability caused by horizontal joints when selecting the optimal mix design.

In this study, mix C1 with a compressive strength of 16.3 MPa was initially selected as the reference criterion. The cohesion-to-compressive strength ratio in non-jointed specimens typically ranges between 0.16 and 0.3, whereas in jointed specimens with bedding mortar, this ratio varies between 0.5 and 1.5. Based on project requirements, a cohesion-to-compressive strength ratio of 1.3 was adopted to ensure optimal bonding performance and resistance to permeability. The mechanical properties and durability parameters of the dam mix design are summarized in Table 6.

Table 6: Mechanical Properties and Durability Targets of the Dam Mix Design.

Variables	Objective	Lower Limit	Upper Limit
Concrete	Maximization	0.536	0.891668
Mortar	Maximization	0.417	0.9153
Time Interval (h)	Maximization	2	48
Compressive Strength	15.4 MPa	11.29	31.9
Tensile Strength	1.26 MPa	0.82	2.16
Cohesion Stress	2.6 MPa	1.25	4.343
Permeability Coefficient	3.0×10^{-10} m/s	1.37×10^{-11}	9.81×10^{-10}

To comprehensively evaluate the mix designs, the signal-to-noise (S/N) ratio was calculated for each variable. The primary goal was to maximize the S/N ratio, as a higher ratio indicates better performance for each factor. Figure S8(a) clearly demonstrates the effect of bedding mortar cement content and time interval

on the S/N ratio for the compressive strength objective in mix C1. As shown, only the use of mortars M2 and M3 in mix C1 can achieve desirable compressive strength. Additionally, a 48-hour time interval has a significantly negative effect on compressive strength. The figure illustrates a sharp decline in the S/N ratio as the time interval increases, particularly at 48 hours. Mortar M3, with a cement content of 550 kg/m³, provides the highest S/N ratio, indicating its superior performance compared to other mortars. If, for practical reasons, the second layer must be placed after 48 hours, the cement content of the mix should be increased to maintain compressive strength at a satisfactory level. Figure S8(b) shows that by increasing the cement content to 160 kg/m³ in mix C2, all three designed bedding mortars can be effectively used. Even with a 48-hour time interval, no significant negative effect on compressive strength is observed. As evident, the S/N ratio curves for all three mortars in mix C2 lie within a higher range than those in mix C1. Even at the 48-hour interval, the S/N ratios for all mortars remain above the acceptable threshold. These results provide greater flexibility in scheduling layer placement and selecting bedding mortar, which is highly valuable for practical RCC dam projects.

Next, the influence of variables on tensile strength was examined. The results indicated that the direct tensile strength of roller-compacted concrete is significantly affected by the relatively coarse aggregate gradation and low paste content present in the mix design. Specifically, the presence of horizontal joints can reduce the tensile strength of specimens by up to approximately 50%. Figure S9(a) shows that even with the use of mortar M3 in mix C1, the desired tensile strength for the dam design cannot be achieved. All curves corresponding to different mortars in this figure lie below the target level for the dam design. Notably, at longer time intervals, a severe decline in the S/N ratio is observed, indicating a substantial reduction in tensile strength. Even in the best scenario (mortar M3 and a 2-hour interval), the S/N ratio does not reach the desired threshold. Therefore, to meet the required tensile strength, the cement content in the concrete mix must be increased. Figure S9(b) demonstrates that by increasing the cement content to 160 kg/m³ in mix C2, the desired tensile strength can be achieved both in the bulk concrete and in the joints. In this figure, the curves for all three mortars at 2- and 12-hour intervals lie above the reference line for the target tensile strength. However, the 48-hour interval still causes a significant drop in tensile strength, with the curves sharply declining below the reference threshold. Hence, when using mix C2, the second layer can be placed at intervals of 2 and 12 hours, and any of the three mortars can be employed effectively.

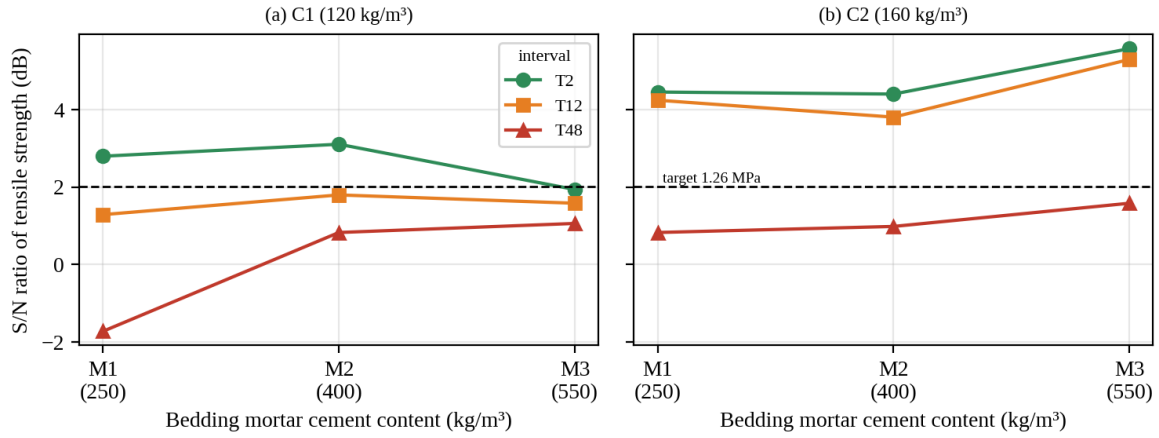


Figure S9: S/N ratio of tensile strength for (a) mix C1 and (b) mix C2 versus bedding mortar cement content and placement interval (data of Table 3; dashed line: design target of Table 6).

Next, the effects of variables on shear strength and joint cohesion were investigated. Figure S10(a) shows that if mix C1 is used for dam construction, adequate cohesion for the design can only be achieved with mortar M3 and a 2-hour time interval. In this figure, only the curve for mortar M3 at the 2-hour interval lies above the reference cohesion line for the dam design. As the time interval increases, all curves rapidly decline below the reference line, indicating a severe reduction in cohesion with increasing time. These limitations suggest that mix C1 offers limited flexibility in achieving the desired shear strength at the joints and is accompanied by significant practical constraints. Figure S10(b) demonstrates that with mix C2, except for mortar M1, cohesion requirements for the dam design can be met in all other cases. The curves for mortars M2 and M3 remain above the reference cohesion line across all time intervals, whereas the curve for mortar M1 lies below the reference line at all intervals. These results indicate that increasing the cement content to 160 kg/m³ enhances the ability to achieve satisfactory joint cohesion even at longer time intervals, thereby providing greater execution flexibility.

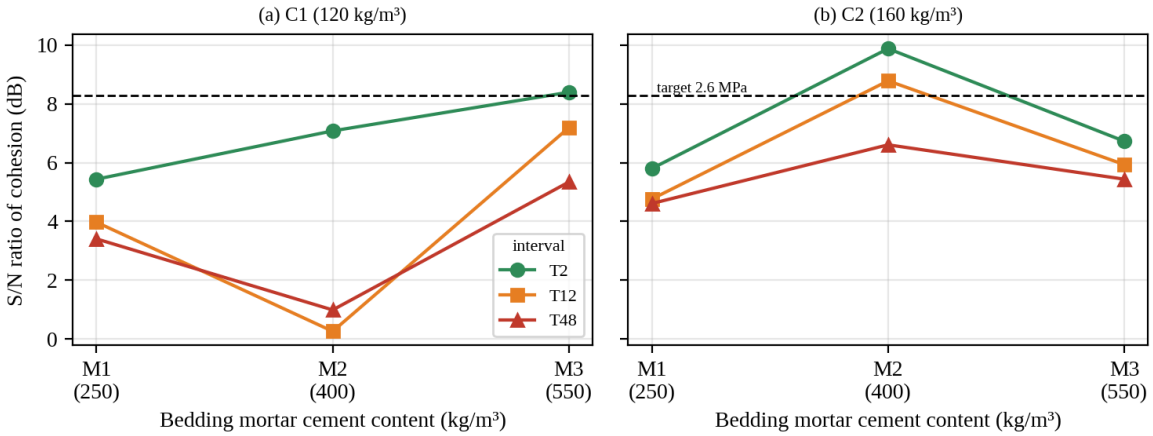


Figure S10: S/N ratio of cohesion for (a) mix C1 and (b) mix C2 versus bedding mortar cement content and placement interval (data of Table 4; dashed line: design target of Table 6).

Permeability is another critical parameter in the design of concrete dams, as dams serve as primary water barriers. To ensure proper dam performance, the permeability coefficient should not exceed 30×10^{-11} m/s. Figure 8(a) shows that, for mix C1, permeability exceeds the acceptable limit under all tested conditions. In this figure, all curves lie below the reference permeability threshold, indicating permeability levels higher than the allowable limit. Even with mortar M3 and the shortest time interval, permeability remains above the desired threshold. These results suggest that mix C1 is insufficient to provide adequate water tightness for the dam and requires modification by increasing the cement content. Figure 8(b) illustrates that increasing the cement content to 160 kg/m³ (mix C2) significantly reduces permeability. In this figure, the curves corresponding to mortars M2 and M3 at 2- and 12-hour intervals lie above the permeability reference line, indicating permeability levels below the permissible limit. By employing mortars M2 and M3 and placing the subsequent layer within 2 to 12 hours, the targeted permeability levels specified by designers can be effectively achieved.

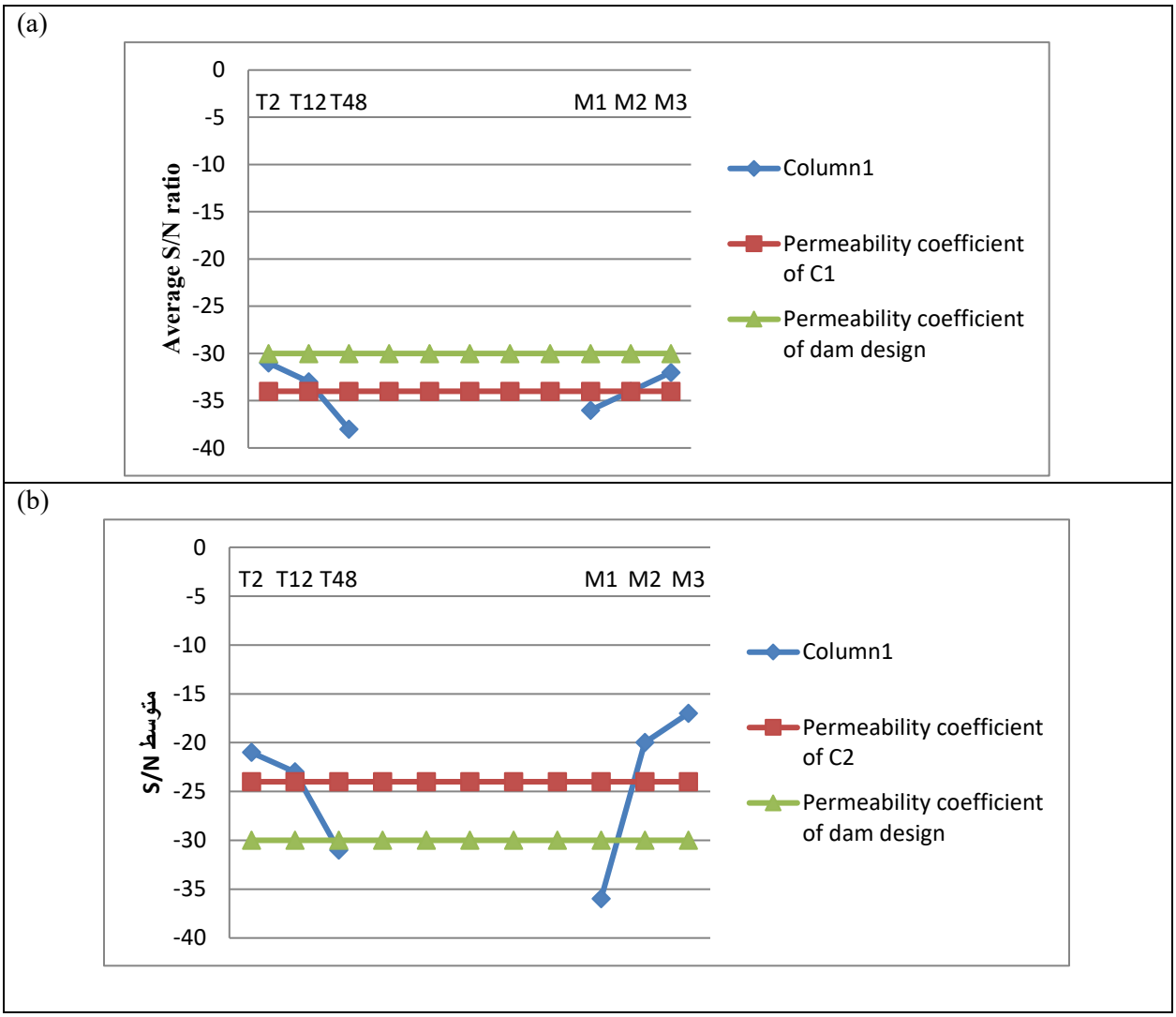


Figure 8: Influence of Bedding Mortar Cement Content and Time Interval on Permeability: (a) Mix C1 and (b) Mix C2.

For the final consolidation and evaluation, the acceptable mix designs based on statistical analyses and the Taguchi method are summarized in Table 7. Table 7 indicates that to simultaneously satisfy all design criteria for the dam, the optimal combination is using mix C2 with a cement content of 160 kg/m³, mortar M2 with a cement content of 400 kg/m³, and a 2-hour time interval between layer placements. This optimal mix provides a balanced compromise between mechanical performance, durability, and economic considerations. Mix C1 is only applicable for compressive strength and even then, with significant limitations, whereas mix C2 demonstrates greater flexibility across all parameters. Mortar M1, with a cement content of 250 kg/m³, is only suitable for tensile strength within mix C2, while mortars M2 and M3 are appropriate for most parameters. Considering economic factors, mortar M2 was selected as the final choice.

Table 7: Mix Designs Obtained by the Taguchi Method.

Property	Concrete Mix	Time Interval	Mortar Mix

Compressive Strength	C1	T2, T12	M2, M3
Tensile Strength	C2	T2, T12	M1, M2, M3
Shear Strength	C1	T2	M3
	C2	T2, T12, T48	M2, M3
Permeability	C2	T2, T12	M2, M3
Final Recommendation	C2 = 160 kg/m³	T2 = 2 hours	M2 = 400 kg/m³

3.5.2. Mathematical Models for Predicting Strength, Permeability, and Mix Optimization

To develop mathematical models for predicting the properties of roller-compacted concrete and optimizing the mix design, multivariate linear regression was employed to relate independent variables (concrete cement content, second layer placement time, and mortar cement content) to laboratory responses. The resulting equations, presented in Equations 6 to 9, provide predictions for compressive strength (F-c), tensile strength (F-t), cohesion stress at the joint (C-p), and permeability coefficient (P-C).

$F_c = 60.97 - 31.86 \times C - 39.8 \times M - 0.15 \times T + 4.5 \times (C \times M) - 0.004 \times (C * T) + 0.022 \times (M \times T) - 1.30 \times C^2 + 18.54 \times M^2 + 0.0016 \times T^2$	(6)
$F_t = 3.67 - 2.55 \times C - 0.99 \times M - 0.040 \times T + 1.00 \times (C \times M) + 0.023 \times (C \times T) - 0.0016 \times (M \times T) + 0.15 \times C\,2 - 0.058 \times M2 + 0.0004 \times T^2$	(7)
$C_p = -0.080 + 1.13 \times C + 0.205 \times M + 0.006 \times T - 0.463 \times (C \times M) + 0.003 \times (C \times T) - 0.0016 \times (M \times T) - 0.36 \times C\,2 + 0.345 \times M2 - 0.00008 \times T^2$	(8)
$\ln PC = -35.4730 + 19.236 \times C + 6.542 \times M + 0.102 \times T - 10.325 \times (C \times M) - 0.06 \times (C \times T) - 0.026 \times (M \times T) - 4.343 \times C\,2 + 3.313 \times M2 - 0.0005 \times T^2$	(9)

In these equations, C represents the concrete cement content, M denotes the mortar cement content, and T signifies the time interval between the placements of the second layer. Quadratic terms (C^2, M^2, T^2) are included to model nonlinear effects, while interaction terms (C×M, C×T, M×T) capture the interplay between variables.

To evaluate the validity and statistical significance of these models, analysis of variance (ANOVA) was performed, with results presented in Table S2. A significance level of 5% ($p < 0.05$) was used to assess model significance. Table S2 displays the ANOVA results for all four models (compressive strength, tensile strength, shear strength, and permeability coefficient). In all cases, p-values were less than 0.05, indicating statistical significance at the 95% confidence level. For compressive strength, the concrete cement content (C) and mortar cement content (M) exert the greatest influence, with F-values of 508.47 and 137.10 respectively, while time interval (T) shows a lesser effect with an F-value of 25.35. This suggests that compressive strength of jointed samples is predominantly influenced by cement content in concrete and mortar, with a relatively minor effect from the second layer placement interval. Regarding tensile strength, time interval (T) has the highest impact with an F-value of 267.30, followed by concrete cement content (C) with an F-value of 134.50. This indicates that tensile strength of joints is highly dependent on the timing of layer placement, and increasing the time interval significantly reduces tensile strength. For shear strength, mortar cement content (M) has the most substantial effect with an F-value of 409.66, followed by concrete

cement content (C) with 318.43 and time interval (T) with 140.98. This highlights that joint shear strength is strongly affected by both mortar and concrete cement contents. Finally, for the permeability coefficient, concrete cement content (C) has the greatest influence (F-value of 144.13), followed by mortar cement content (M) (103.45) and time interval (T) (81.02). This suggests that joint permeability is primarily governed by the cement contents of concrete and mortar, with time interval being less influential.

After identifying the most significant variables, a refined regression model was developed including only these factors. The general form of this regression is presented in Equation 10.

$$F = C + X1(C) + X2(M) + X3(T) + X4(C \times M) + X5(C \times T) + X6(M \times T) + X7(C \times C) + X8(M \times M) + X9(T \times T) \quad (10)$$

The coefficients of the general regression equation for each roller-compacted concrete property are presented in Table 8.

Table 8: Coefficients of the General Regression Equation

Variables	Coefficients (X)	F: Concrete Property			
		Compressive Strength	Tensile Strength	Cohesion Stress	Permeability Coefficient
Constant	C	60.95466	3.6557	0.07856	-35.4730
C	X1	-31.8446	-2.5357	1.1202	19.2349
M	X2	-39.70036	-0.9850	0.2038	6.5412
T	X3	-0.138637	-0.0388	0.0048	0.1011
C×M	X4	-	0.9994	-0.4620	-10.3241
C×T	X5	-	0.0216	-	-0.0505
M×T	X6	-	-	-0.00154	-
C^2	X7	-	-	-	-
M^2	X8	18.52875	-	0.3436	-
T^2	X9	-	0.00026	-0.00008	-

Table 8 shows that some terms have been omitted in certain models (indicated by "-") due to their lack of statistical significance on the responses. The coefficients of determination (R^2) for the compressive strength, tensile strength, shear strength, and permeability models were 0.96, 0.97, 0.98, and 0.99, respectively, indicating a strong correlation between the predictor variables and model responses.

To better understand the simultaneous effects of variables on different responses, response surface plots were generated. Figure S11 illustrates the response surface diagrams for the compressive and tensile strength models. Figures S11(a) to S11(c) depict variations in compressive strength of roller-compacted concrete specimens while keeping the concrete cement content constant and varying the mortar cement content and time interval. These figures clearly demonstrate that using mortar with higher compressive strength (i.e., higher cement content) increases specimen strength, whereas increasing the time interval between layer placements gradually reduces compressive strength. The steep slope of the response surface along the mortar cement content axis highlights the significant influence of this variable on compressive strength. Figures S11(d) to S11(f) show the combined effect of mortar cement content and time interval on the tensile strength of jointed specimens. It is evident that reducing the time interval between layers significantly enhances tensile strength, while increasing the water-to-cement ratio of the mortar causes a

gradual decline in tensile strength. The very steep slope of the surface along the time axis emphasizes the high sensitivity of tensile strength to the timing of layer placement.

Figures S12(a) to S12(c) illustrate the variations in shear strength of the joints in the specimens. These figures show that reducing the time interval between layer placements significantly increases the shear strength. However, the effect of time on shear strength varies depending on the concrete cement content. At higher water-to-cement ratios (lower cement content), the influence of time on shear strength is less pronounced, and in this case, the intrinsic shear strength of the concrete itself primarily governs the shear behavior. Conversely, at lower water-to-cement ratios (higher cement content), the effect of time on shear strength becomes more significant. Figures S12(d) to S12(f) present variations in the permeability coefficient. These figures clearly indicate that mortar cement content has a greater impact on joint permeability compared to time. Additionally, joints covered with mortar having a high water-to-cement ratio (0.93) are more affected by time than those with mortar having a low water-to-cement ratio (0.43). This finding suggests that using mortar with high cement content and minimizing the time interval for placing the second layer are highly effective strategies for significantly reducing joint permeability.

3.5.3. Multivariate Optimization Using Response Surface Methodology

To identify the optimal combination of concrete cement content, mortar cement content, and second layer placement time that meets the target strength and permeability, response surface methodology (RSM) was employed. To validate the optimization results, new specimens were prepared and tested according to the optimal mix design. The validation results are summarized in Table 9.

Table 9: Parameter Values and Obtained Responses.

Variables	Optimal Mix Design and Predictions	Experimental Results	Error (%)
Concrete	0.893	—	—
Mortar	M2 < 0.618 < M1	—	—
Time Interval (h)	2	—	—
Compressive Strength (MPa)	16.268	15.10	7.7
Tensile Strength (MPa)	1.387	1.32	5.1
Cohesion Stress (MPa)	2.333	2.3	1.4
Permeability Coefficient (m/s)	2.99×10^{-10}	3.41×10^{-10}	12.3

Table 9 shows that the predictions of the mathematical models agree well with the results of the validation tests. The prediction errors for compressive strength, tensile strength, cohesion and permeability coefficient were 7.7%, 5.1%, 1.4% and 12.3%, respectively. The larger error for permeability is expected, because the permeability coefficient spans almost two orders of magnitude in the data set and was modelled on a logarithmic scale; an error of 12.3% in k corresponds to an error of less than 1% in ln k. All errors are within the range usually considered acceptable for concrete property models, which confirms that the models can be used for design-level prediction within the tested domain.

The comparison between the optimal mix designs obtained from the Taguchi analysis and response surface methodology (RSM) indicates that the Taguchi method provides more conservative results, as it selects the optimal mix only from the existing designed mixtures. In contrast, the RSM, by utilizing more precise mathematical relationships between variables, can propose an optimal point even beyond the range of the tested mixtures. The optimal design derived from the RSM specifies a concrete cement content of 0.893

(close to mix C2), a mortar cement content between M1 and M2 (0.618), and a time interval of 2 hours. This combination results in a compressive strength of 16.268 MPa, tensile strength of 1.387 MPa, cohesion stress of 2.333 MPa, and a permeability coefficient of 2.99×10^{-10} m/s-all within the desirable design range. These findings demonstrate that the response surface method can serve as an effective tool for optimizing multiple parameters in roller-compacted concrete mix design, leading to material savings and cost reductions while maintaining the targeted mechanical properties and durability.

3.5.4. Fuzzy Multi-Response Performance Index

The fuzzy inference procedure of Section 2.8 was applied to the 27 factor combinations using joint tensile strength, joint cohesion and permeability coefficient as inputs. Table 10 lists the combinations with the highest MRPI values together with the recommended combination, and Table 11 gives the mean MRPI of each factor level and the percentage contribution of each factor. The membership functions of the fuzzy system and the factor-level means of the MRPI are plotted in Figure 9.

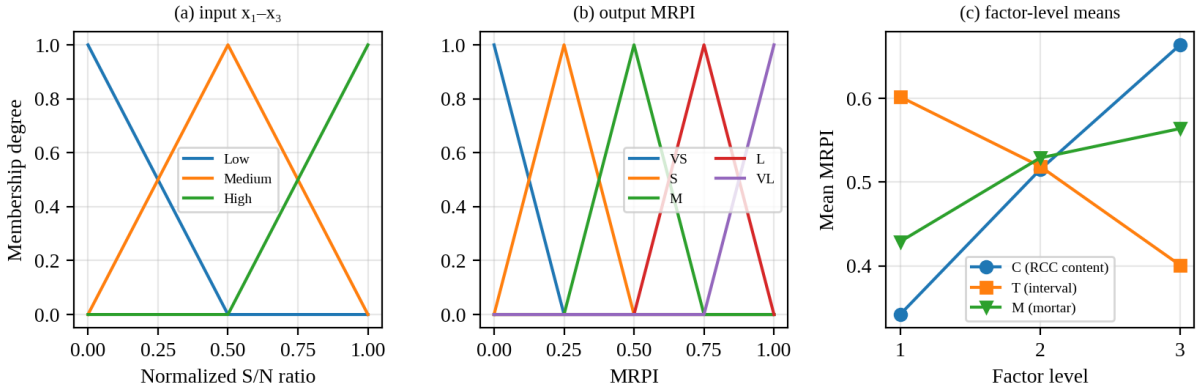


Figure 9: Fuzzy multi-response performance index: (a) input and (b) output membership functions defined in Section 2.8; (c) mean MRPI at each factor level (Table 11).

Table 10: Normalized S/N Ratios and Fuzzy MRPI of Selected Combinations.

Run	x_1 (tensile)	x_2 (cohesion)	x_3 (permeability)	MRPI	Rank
C3M2T2	0.862	1.000	0.987	0.818	1
C3M3T2	1.000	0.860	1.000	0.817	2
C3M2T12	0.966	0.883	0.839	0.774	3
C3M3T12	0.624	0.848	0.900	0.695	4
C3M1T2	0.771	0.958	0.459	0.665	5
C2M3T2	0.868	0.521	0.775	0.665	6
C2M2T2	0.728	0.776	0.728	0.660	7

Table 11: Mean MRPI at Each Factor Level and Percentage Contribution of Factors.

Factor	Level 1	Level 2	Level 3	Δ (max − min)	Contribution (%)	Rank

RCC cementitious content (C)	0.342	0.515	0.664	0.322	59.3	1
Placement interval (T)	0.602	0.519	0.401	0.200	23.2	2
Mortar cement content (M)	0.429	0.529	0.564	0.135	11.2	3
Residual (interactions)	—	—	—	—	6.3	—

Three findings emerge from the fuzzy analysis. First, the RCC cementitious content is the most influential factor for the combined joint performance (59.3%), followed by the placement interval (23.2%) and the mortar cement content (11.2%); the remaining 6.3% is attributable to interactions. This ranking differs from the single-response analyses, in which the interval dominated tensile strength and the mortar dominated cohesion, and it shows that improving the parent concrete raises all three responses simultaneously. Second, the MRPI of C3M2T2 (0.818) is practically equal to that of C3M3T2 (0.817), and the mean MRPI of the M2 level (0.529) is only 6% lower than that of M3 (0.564); increasing the mortar cement content from 400 to 550 kg/m^3 therefore yields almost no multi-response benefit, because the additional cement improves permeability but not cohesion. Third, the MRPI decreases monotonically with the placement interval, and the reduction between 12 and 48 h (0.118) is larger than between 2 and 12 h (0.083), which confirms that exceeding the final setting time is the most damaging scheduling decision.

The fuzzy analysis identifies C3M2T2 as the performance-maximizing combination, whereas the conventional Taguchi and RSM analyses recommend C2M2T2. The two results are complementary rather than contradictory: C2M2T2 is the combination with the lowest total cement consumption that satisfies all the design targets of Table 6 (tensile strength 1.66 MPa ≥ 1.26 MPa, cohesion 3.12 MPa ≥ 2.6 MPa and permeability 4.37×10^{-11} m/s ≤ 30×10^{-11} m/s), and it ranks seventh of 27 in MRPI. By contrast, C2M3T2 has a similar MRPI (0.665) but fails the cohesion target (2.17 MPa), which demonstrates that a high aggregated index alone is not a sufficient selection criterion and that the explicit constraint check of the RSM–desirability stage is necessary. The two-stage framework therefore separates the question 'which combination performs best?' from 'which is the most economical combination that is good enough?', and this distinction is directly useful when cement availability, heat of hydration or cost constrain the design.

From a construction standpoint, the results support an interval-based joint classification. Lifts placed before the initial set of the lower lift (2 h) form hot joints that require only surface cleaning and a moderate-strength bedding mortar; lifts placed between initial and final set (up to 12 h) remain acceptable with the M2 mortar provided that the RCC contains at least 160 kg/m^3 of cementitious material; lifts placed after final set (48 h) behave as cold joints that cannot meet the tensile and permeability targets with any of the tested mortars and therefore require additional surface preparation, such as green cutting or high-pressure water-jetting, before the mortar is placed. These limits are expressed relative to the setting times and can be transferred to other mixtures if their setting times are measured.

The study has limitations that should be considered when the results are applied. The tests were performed on laboratory specimens compacted with a vibrating hammer, which may not reproduce the compaction energy, segregation and lift-surface conditions of full-scale roller compaction; freeze–thaw, leaching, sulphate and high-temperature durability were not measured directly [20, 31]; all specimens were cured in water at 23 ± 2 °C for 90 days, whereas field joints are exposed to variable temperature and moisture; and a single aggregate source and fly ash were used. Field trial sections with cored specimens and long-term durability tests are needed to extend the framework.

4. Conclusion and Recommendations

This study investigated the lift joints of roller-compacted concrete dams through a 3^3 full-factorial programme of 30 runs and 300 specimens in which the RCC cementitious content (120, 160 and 200 kg/m^3), the bedding-mortar cement content (250, 400 and 550 kg/m^3) and the placement interval (2, 12 and 48 h) were varied, and it proposed a two-stage optimization framework combining a fuzzy multi-response Taguchi analysis with RSM-based desirability optimization. The main conclusions are as follows.

(1) The placement interval relative to the setting times of the lower lift is the dominant factor for joint tensile strength (F = 267.3). Jointed specimens retained about 90%, 84% and less than 60% of the monolithic direct tensile strength (1.52, 1.90 and 2.40 MPa for C1, C2 and C3) at intervals of 2, 12 and 48 h, respectively, and the failure plane moved from the mortar or parent concrete to the interface between the mortar and the lower lift once the initial set was exceeded.

(2) In the Mohr–Coulomb representation of joint shear strength, the friction coefficient remained practically constant (≈1.1–1.4), whereas cohesion increased by more than 1.5 times from C1 to C3 and was on average 88% higher for hot joints than for cold joints. The bedding-mortar cement content was the most influential factor for cohesion (F = 409.7), and the effect of placement delay should be introduced in stability analyses mainly through the cohesion term.

(3) Increasing the RCC cementitious content from 120 to 200 kg/m^3 reduced the permeability coefficient of unjointed concrete by about 90% (from $\approx 45\times10^{-11}$ to $<5\times10^{-11}$ m/s). Increasing the mortar cement content from 250 to 550 kg/m^3 reduced the joint permeability of C3T2 specimens by about 85%, but the jointed specimens remained more permeable than the parent concrete, so the joint remains the controlling seepage path. Capillary absorption and pressure permeability were strongly correlated ($R^2 \approx 0.92$), so the simpler sorptivity test can be used for quality control.

(4) The fuzzy MRPI attributed 59.3%, 23.2% and 11.2% of the combined joint performance to the RCC cementitious content, the placement interval and the mortar cement content, respectively. The best-performing combination was C3M2T2 (MRPI = 0.818), practically identical to C3M3T2 (0.817), which shows that mortar richer than 400 kg/m^3 brings no multi-response benefit.

(5) Second-order regression models for compressive strength, tensile strength, cohesion and permeability achieved R^2 values of 0.96, 0.97, 0.98 and 0.99 and predicted independent validation tests with errors of 7.7%, 5.1%, 1.4% and 12.3%, respectively. The Taguchi analysis, restricted to the tested levels, gave more conservative recommendations than RSM, which can locate optima between the tested levels.

(6) The minimum-cement combination that satisfies all design targets is an RCC with 160 kg/m^3 cementitious material (30% fly ash), a bedding mortar with 400 kg/m^3 cement and placement of the next lift within 2 h, with 12 h as an upper limit. This combination saves 40 kg/m^3 of cementitious material in the RCC body and 150 kg/m^3 of cement in the mortar compared with the performance-maximizing combination while still meeting the strength and permeability requirements.

4.1 Practical Recommendations

For RCC dam projects with materials similar to those used here, it is recommended that: (a) the cementitious content of the RCC be not less than 160 kg/m^3 with about 30% fly ash, since the leanest mixture failed the tensile, cohesion and permeability targets regardless of the mortar used; (b) the next lift be placed before the initial set of the lower lift (2 h in this study), and that 12 h be treated as an upper limit that requires bedding mortar; (c) joints older than the final setting time be treated as cold joints that need surface

preparation before a bedding mortar with about 400 kg/m^3 cement is placed; (d) the setting times of each production mixture be measured so that placement limits can be expressed relative to them; and (e) the regression models and the fuzzy MRPI be used during the design phase to evaluate alternative mixtures and schedules before trial sections are built.

4.2 Research Recommendations

- Investigate the effects of nanomaterials and microsilica additives on RCC mechanical properties and durability.
- Evaluate the use of recycled materials (e.g., crushed glass, rubber) in RCC mix designs.
- Compare RCC performance under harsh environmental conditions such as freeze-thaw cycles, acid rain, and chemical attacks.
- Conduct more detailed studies on RCC service life and the impact of execution and design parameters.

Reference

1. Abed, Z., H. Ahmed, and W. Khalil, *Optimization of silica fume and slag in roller compacted concrete by Taguchi method.* Engineering and Technology Journal, 2023. **41**(05): p. 724-733.
2. Adamu, M., et al., *Multicriteria-based optimization of roller compacted concrete pavement containing crumb rubber and nano-silica.* Nanotechnology Reviews, 2024. **13**(1): p. 20240046.
3. Aniskin, N.A. and A.M. Shaytanov, *Optimization of the temperature and thermo-stressed state of a concrete dam constructed from particularly lean roller-compacted concrete.* Buildings, 2023. **13**(4): p. 914.
4. Chakali, Y., et al., *A PSO-ANN intelligent hybrid model to predict the compressive strength of limestone fillers roller compacted concrete (RCC) to build dams.* KSCE Journal of Civil Engineering, 2021. **25**(8): p. 3008-3018.
5. Habib, A., et al., *Structural performance and Finite Element modeling of roller compacted concrete dams: A review.* Latin American Journal of Solids and Structures, 2021. **18**(04): p. e376.
6. Khan, M.A., et al., *Simulation of depth of wear of eco-friendly concrete using machine learning based computational approaches.* Materials, 2021. **15**(1): p. 58.
7. Pei, L., et al., *System reliability of a gravity dam-foundation system using Bayesian networks.* Reliability Engineering & System Safety, 2022. **218**: p. 108178.
8. Sobhkhiz Foumani, R., A. Mardookhpour, and F. Saberi, *Optimization of time and temperature of dam construction for thermal analysis of roller compacted concrete dam.* Numerical Methods in Civil Engineering, 2023. **7**(4): p. 1-11.
9. Warda, M.A., et al., *The applicability of TOPSIS-and fuzzy TOPSIS-based Taguchi optimization approaches in obtaining optimal fiber-reinforced concrete mix proportions.* Buildings, 2022. **12**(6): p. 796.
10. Zhuo, M.-Y., et al., *Seepage Prediction Model for Roller-Compacted Concrete Dam Using Support Vector Regression and Hybrid Parameter Optimization.* Water, 2023. **15**(19): p. 3511.
11. Asthana, B. and D. Khare, *Roller compacted concrete dams*, in *Recent Advances In Dam Engineering*. 2022, Springer. p. 73-88.
12. Jin, F., et al., *A brief review of rock-filled concrete dams and prospects for next-generation concrete dam construction technology.* Engineering, 2024. **32**: p. 99-105.
13. Jin, J., et al., *Seepage Mitigation in Hydropower Dams by Optimization in Roller Compacted Concrete Interlayer (Monoliths) Joint Bonding Technology.* Open Journal of Civil Engineering, 2022. **12**(1): p. 139-151.

14. Mirković, U., V. Kuzmanović, and G. Todorović, *Long-Term Thermal Stress Analysis and Optimization of Contraction Joint Distance of Concrete Gravity Dams.* Applied Sciences, 2022. **12**(16): p. 8163.
15. Ojhaa, P., et al., *Effect of high ratio fly ash on roller compacted concrete for dam construction.* Research on Engineering Structures and Materials, 2022. **8**(2): p. 233-251.
16. Satish, B.J.N., et al., *Design optimization of non-overflow section of a concrete gravity dam.* Journal of Building Pathology and Rehabilitation, 2022. **7**(1): p. 31.
17. Singh, B., et al., *Cost optimization of RCC column using discrete optimisation method.* Materials Today: Proceedings, 2022. **48**: p. 1390-1394.
18. Şermet, F., et al., *The effect of the gravity on the earthquake performance of roller compacted concrete dams.* Challenge Journal of Concrete Research Letters, 2024. **15**(1): p. 20-29.
19. Sheelavantar, P.G., et al., *Taguchi-integrated grey relational analysis for multi-response optimization of mix design for alkali-activated concrete.* Materials Research Express, 2024. **11**(7): p. 075505.
20. Lyu, C., et al., *Long-term performance and microstructural characterization of dam concrete in the three gorges project.* Engineering, 2024. **33**: p. 237-262.
21. Kantasiri, T., et al., *Optimization of concrete containing waste crumb rubber mix design for thermal insulating applications using Taguchi method.* Construction and Building Materials, 2024. **434**: p. 136636.
22. Bayqra, S.H.; Özen, S.; Mardani, A.; Ramyar, K., *Effect of interlayer cold joint on mechanical properties and permeability of roller compacted concrete.* Frontiers of Structural and Civil Engineering, 2025. 19(2): p. 284–299. https://doi.org/10.1007/s11709-025-1145-z
23. Hao, C.; He, X.; Liu, N.; Wang, J., *Application Research of Maturity Indicators in Interlayer Quality Control of Roller-Compacted Concrete Dams: A Case Study of the Kafue Gorge Lower Hydropower Station in Zambia.* Applied Sciences, 2026. 16(10): p. 5123. https://doi.org/10.3390/app16105123
24. Han, R.; Hao, Y.; He, S.; Jin, R.; He, D.; Zhang, M.; Wang, Q., *Theoretical Calculation of RCC Layer Thickness Based on Equivalent Elastic Model and Numerical Study on Dam Deformation.* Buildings, 2026. 16(6): p. 1186. https://doi.org/10.3390/buildings16061186
25. Ramadan, M.; Jia, J.; Zhao, L.; Li, X.; Wu, Y., *Numerical and Fracture Mechanical Evaluation of Safety Monitoring Indexes and Crack Resistance in High RCC Gravity Dams Under Hydraulic Fracture Risk.* Materials, 2025. 18(12): p. 2893. https://doi.org/10.3390/ma18122893
26. Lee, J.-C., *Optimization of Mix Design for Lightweight Boards Based on GGBFS–Waste Rock Wool Using Response Surface Methodology.* Materials, 2025. 18(23): p. 5376. https://doi.org/10.3390/ma18235376
27. Jagadisha, H.M.; Pandit, P.; Prashant, S.; Bhole, L.; Singh, Y.; Verma, O.; Kumar, M., *Multi-objective Optimisation of One-Part Slag–Flyash–Microsilica Based Alkali-Activated Ternary Binder Mixes.* International Journal of Concrete Structures and Materials, 2025. 19(1): p. 75. https://doi.org/10.1186/s40069-025-00822-z
28. Raman, S.; Nateriya, R., *Sustainable Granite Powder Concrete Development Through Taguchi-Based Multi-response Optimization: A Moisture Correction Framework for Enhanced Performance.* Journal of Inorganic and Organometallic Polymers and Materials, 2025 (published online 16 July 2025). https://doi.org/10.1007/s10904-025-03945-8
29. Murugan, A.; Barik, D.; Faisal, R.S.; Mani, M.; Dennison, M.S.; Praveenkumar, S.; Rajendran, S., *Optimization of tribo-mechanical properties of kenaf/jute-SiC hybrid composites using integrated grey-fuzzy approach.* Scientific Reports, 2025. 15. https://doi.org/10.1038/s41598-025-11340-z
30. Ahıskalı, M.; Bayraktar, O.Y.; Ahıskalı, A.; Benli, A.; Kaplan, G., *Eco-efficient roller-compacted concrete with recycled aggregates and fiber reinforcement.* Sustainable Chemistry and Pharmacy, 2025. 48: p. 102246. https://doi.org/10.1016/j.scp.2025.102246

31. Ünverdi, M.; Kaya, Y.; Mardani, N.; Mardani, A., *Investigation of the Microstructural and Mechanical Properties of Fiber-Reinforced Roller-Compacted Concrete Under High-Temperature Exposure.* Materials, 2025. 18(11): p. 2430. https://doi.org/10.3390/ma18112430